On the generation of homogeneous, inhomogeneous and Goodier–Bishop elastic waves from the geometrical ray theory

Article *in* Journal of Engineering and Applied Sciences · May 2015

CITATIONS
3

READS
105

2 authors, including:

Victor Hugo Aristizabal
Universidad Cooperativa de Colombia
37 PUBLICATIONS **105** CITATIONS

SEE PROFILE

VOL. 10, NO. 8, MAY 2015 ISSN 1819-6608
ARPN Journal of Engineering and Applied Sciences

www.arpnjournals.com

ON THE GENERATION OF HOMOGENEOUS, INHOMOGENEOUS AND GOODIER-BISHOP ELASTIC WAVES FROM THE GEOMETRICAL RAY THEORY

Victor H. Aristizabal[1, 2] and Juan D. Jaramillo[1]
[1]Department of Civil Engineering, EAFIT University, Medellín, Colombia
[2]School of Engineering, Cooperative University of Colombia, Medellín, Colombia
E-Mail: vharisti@yahoo.com

ABSTRACT

In this paper, a new group of exact and asymptotic analytical solutions of the displacement equation in a homogeneous elastic media, considering the most general solution of the Helmholtz equation, which have not been shown in papers and standard texts, are presented. Moreover, the authors show from the ray theory point of view the meaning of such solutions. These solutions could be helpful in future conceptual works about generation and emerging phenomena in elastic waves such as scattering and diffraction, among others, specifically in the analysis of the boundary conditions. Here, new kinds of P-S body waves that oscillate elliptically and propagate outward from sources in a full-space are found where, as special cases, the grazing longitudinal (*P*y) and transversal (*SV*y) waves of the Goodier-Bishop type, the analytic expressions for the Rayleigh wave and surface P waves, for which the amplitude decays from sources, are obtained. Also, the standard expressions for the homogeneous plane wavefronts, surface *P* waves, and Rayleigh surface waves, are achieved.

Keywords: elastic waves, seismic wave, displacement equation, analytical solutions, Goodier-Bishop waves, Helmholtz equation.

1. INTRODUCTION

In elastodynamics the exact solutions available are limited; therefore it is necessary to either use different approximate methods or to modify the problem in a way that it can be described in terms of fundamental known solutions. Such solutions are usually obtained from the propagation of secondary horizontal (*SH*) waves on special geometries [1-7]. Solving problems involving primary (*P*), secondary vertical (*SV*) and surface waves is more difficult due to the coupling of the field components either in the displacement equation or in the boundary conditions. Lee [8, 9] overcame that inconvenience with a hemispherical valley and canyon expansion into spherical Bessel functions and Legendre polynomials, resulting in a match for all the boundary conditions; and Todorovska and Lee [10] proposed a solution fora circular valley by Fourier-Bessel series expansion.

In spite of the limitations regarding analytical methods and advances in numerical approximations applicable to arbitrary shapes and in homogeneities, the analytical solutions are still essential to test the numerical methods. Furthermore they allow for a physical understanding when identifying dominating parameters in the problems under observation. In fact, these are the main reasons for seeking fundamental solutions to the displacement equation.

This work presents *P-SV* elementary wavefronts and their sources in order to conceptualize their behavior in anisotropic, homogeneous and linear elastic medium. These solutions could be helpful in future conceptual works about diffraction, scattering and generation of elastic waves; specifically when satisfying the boundary conditions.

2. BASIC EQUATIONS

Equations governing linearized elastodynamics of a homogeneous isotropic medium are briefly summarized here. More details can be found in [11]. The theory begins with the displacement equation in absence of body forces for an isotropic, homogeneous and linear elastic medium:

$$(\lambda+\mu)\vec{\nabla}\vec{\nabla}\cdot\vec{u}+\mu\nabla^2\vec{u}=\rho\ddot{\vec{u}}, \quad (1)$$

Where λ and μ are the Lamé parameters of the medium and ρ is its mass density.

The direct solution of Equation (1) is difficult to obtain due to the fact that the displacement components are coupled. A more convenient way is to express the displacement field in terms of a scalar potential φ and a vector potential $\vec{\psi}$:

$$\vec{u}=\vec{\nabla}\varphi+\vec{\nabla}\times\vec{\psi}. \quad (2)$$

It can be shown that the representation in (2) satisfies (1), if φ and $\vec{\psi}$ depend on the form $e^{\pm i\omega t}$ and fulfill the Helmholtz equation:

$$\nabla^2\varphi+k_p^2\varphi=0,$$
$$\nabla^2\vec{\psi}+k_s^2\vec{\psi}=0, \quad (3)$$
$$\vec{\nabla}\cdot\vec{\psi}=0,$$

being $k_p = \omega/c_p$ and $k_s = \omega/c_s$ the wave numbers, where ω is the angular frequency, ${c_p}^2 = (\lambda + 2\mu)/\rho$ and ${c_s}^2 = \mu/\rho$ are the velocities of primary and secondary waves in the medium, respectively. The time factors $e^{\pm i\omega t}$ will be omitted here and thereafter. Note that in later sections it should be taken $e^{-i\omega t}$ for fields with $H_\eta^{(1)}$ and $e^{i\omega t}$ for fields with $H_\eta^{(2)}$ in order to correspond to sources that radiate outward. Although the equations in (3) are uncoupled, the potentials are coupled by means of the boundary conditions which are the main difficulty insolving elastodynamic problems.

3. FUNDAMENTAL SOLUTIONS

Taking ascalar function $\xi(r,\phi)$ in polar coordinates that fulfills the Helmholtz equation:

$$\frac{\partial^2\xi}{\partial r^2} + \frac{1}{r}\frac{\partial\xi}{\partial r} + \frac{1}{r^2}\frac{\partial^2\xi}{\partial\phi^2} + k^2\xi = 0 \quad , \tag{4}$$

where k is the wavenumber; then using the classical method of separation of variables where $\xi(r,\phi) = R(r)\Phi(\phi)$ is substituted in equation (4), two ordinary differential equations are obtained. Supposing that $\xi(r,\phi) \neq 0$ in the work space and manipulating the algebra:

$$\frac{d^2\Phi}{d\phi^2} + \eta^2\Phi = 0 \quad , \tag{5}$$

$$\frac{d^2R}{d\Lambda^2} + \frac{1}{\Lambda}\frac{dR}{d\Lambda} + \left(1 - \frac{\eta^2}{\Lambda^2}\right)R = 0 \quad , \tag{6}$$

with $\Lambda = kr$ being a complex number in general. Equation (5) has solutions in the form:

$$\Phi = \begin{cases} A_0\phi + B_0 & \text{for } \eta = 0; \\ A_\eta\cos\eta\phi + B_\eta\sin\eta\phi & \\ \text{or} & \text{for } \eta \neq 0 \\ A_\eta e^{i\eta\phi} + B_\eta e^{-i\eta\phi} & \end{cases} \tag{7}$$

and equation (6) is the well-known differential equation satisfied by the Bessel functions [12]:

$$R = \begin{cases} C_\eta J_\eta(\Lambda) + D_\eta Y_\eta(\Lambda) & \\ \text{or} & \text{for all values of } \eta \\ C_\eta H_\eta^{(1)}(\Lambda) + D_\eta H_\eta^{(2)}(\Lambda) & \end{cases} \tag{8}$$

where J_η and Y_η are the Bessel functions and $H_\eta^{(1)}$ and $H_\eta^{(2)}$ are the Hankel functions. The most general solution for (4) can be represented by:

$$\xi(r,\phi) = \left[C_0H_0^{(1)}(kr) + D_0H_0^{(2)}(kr)\right](A_0\phi + B_0) + \sum_{\eta\neq 0}\left(C_\eta H_\eta^{(1)}(kr) + D_\eta H_\eta^{(2)}(kr)\right)\left(A_\eta\cos\eta\phi + B_\eta\sin\eta\phi\right) \quad . \tag{9}$$

The functions that could be selected for $\xi(r,\phi)$, taking in mind(7) and (8),depend on the problem under study. The separation constant η, and the constants A_0, B_0, C_0, D_0, A_η, B_η, C_η, D_η are determined from the boundary conditions. For example, in [1, 2] can be seen that $\eta = 2n$ and $2n+1$, in [3, 4] $\eta = n$ and $n+1$, in [5] $\eta = n/\nu$, in [6, 7, 10] $\eta = n$ and in [8, 9] $\eta = n + 1/2$ (spherical Bessel Functions); where $n = 0, 1, 2 \ldots$ and $0 \leq \nu \leq 2\pi$.

It is important to notice that in the above works and standard literature [14-16], the term $A_0\phi$ is not considered without any apparent justification. However, in the following sections the terms $H_0^{(1,2)}(\Lambda)[A_0\phi + B_0]$ are studied from a mathematical, geometrical and physical point of view; which could be essential in the development of new analytical solutions to problems of *P*-*S* waves.

4. LINE SOURCES AND HOMOGENEOUS AND INHOMOGENEOUS CYLINDRICAL WAVEFRONTS

Taking into account the description of the displacement field in terms of potentials for primary (*P*) and secondary (*S*) waves; the authors propose cylindrical potentials, for $0 \leq \phi \leq \nu$ and $r \geq 0$ with $0 \leq \nu \leq 2\pi$, in the form:

$$\varphi^c = -\frac{1}{ik_p}H_0^{(2)}(k_pr)[A\phi + B] \quad ,$$
$$\vec{\psi}^c = \psi_z^c\hat{z} = \frac{1}{ik_s}H_0^{(2)}(k_sr)[C\phi + D]\hat{z} \quad , \tag{10}$$

where A, B, C, D are in general complex constants and $H_0^{(2)}$ is the Hankel function of second kind and zero order. Note that if A and B, C and D are not simultaneously zero; then ψ_z^c and φ^c fulfill (3) except in $r = 0$ where are singular. Then can be written more conveniently as:

$$\nabla^2\varphi^c + k_p^2\varphi^c = \delta(r)/r \quad ,$$

$$\nabla^2\psi_z^c + k_s^2\psi_z^c = \delta(r)/r,$$
$$\nabla\cdot\vec{\psi}^c = 0,$$

Representing harmonic line sources located at $r = 0$.

Now, taking (2) in polar coordinates and

$$\frac{dH_0^{(2)}(\Lambda)}{d\Lambda} = -H_1^{(2)}(\Lambda), \quad (11)$$

the next *P* and *S* fields are obtained

$$\vec{u}_P^c = \nabla\varphi^c = \frac{\partial\varphi^c}{\partial r}\hat{r} + \frac{1}{r}\frac{\partial\varphi^c}{\partial\phi}\hat{\phi}$$
$$= \frac{B}{i}H_1^{(2)}(k_p r)\hat{r} + \frac{A}{i}\left[\phi H_1^{(2)}(k_p r)\hat{r} - \frac{1}{k_p r}H_0^{(2)}(k_p r)\hat{\phi}\right],$$

$$\vec{u}_s^c = \nabla\times\vec{\psi}^c = \frac{1}{r}\frac{\partial\psi_z^c}{\partial\phi}\hat{r} - \frac{\partial\psi_z^c}{\partial r}\hat{\phi}$$
$$= \frac{D}{i}H_1^{(2)}(k_s r)\hat{\phi} + \frac{C}{i}\left[\frac{1}{k_s r}H_0^{(2)}(k_s r)\hat{r} + \phi H_1^{(2)}(k_s r)\hat{\phi}\right]. \quad (12)$$

Furthermore, taking into account the approximation for large Λ in (12) [12]:

$$H_1^{(2)}(\Lambda) \approx iH_0^{(2)}(\Lambda), \quad (13)$$

it is obtained that

$$\vec{u}_P^c \approx \vec{u}_L^c + \vec{u}_P^{ce},$$
$$\vec{u}_s^c \approx \vec{u}_T^c + \vec{u}_s^{ce},$$

where

$$\vec{u}_L^c \equiv BH_0^{(2)}(k_p r)\hat{r},$$
$$\vec{u}_T^c \equiv DH_0^{(2)}(k_s r)\hat{\phi},$$
$$\vec{u}_P^{ce} \equiv AH_0^{(2)}(k_p r)\left[\phi\hat{r} + \frac{i}{k_p r}\hat{\phi}\right], \quad (14)$$
$$\vec{u}_s^{ce} \equiv CH_0^{(2)}(k_s r)\left[-\frac{i}{k_s r}\hat{r} + \phi\hat{\phi}\right].$$

If the following asymptotic expansion of $H_0^{(2)}(\Lambda)$ for large Λ is considered in (14) [12]:

$$H_0^{(2)}(\Lambda) \approx \sqrt{\frac{2}{\pi\Lambda}}e^{i\pi/4}e^{-i\Lambda}, \quad (15)$$

it is finally achieved that

$$\vec{u}_L^c \approx \frac{B_0}{\sqrt{k_p r}}e^{-ik_p r}\hat{r},$$
$$\vec{u}_T^c \approx \frac{D_0}{\sqrt{k_s r}}e^{-ik_s r}\hat{\phi},$$
$$\vec{u}_P^{ce} \approx \frac{A_0}{\sqrt{k_p r}}e^{-ik_p r}\left[\phi\hat{r} + \frac{i}{k_p r}\hat{\phi}\right], \quad (16)$$
$$\vec{u}_s^{ce} \approx \frac{C_0}{\sqrt{k_s r}}e^{-ik_s r}\left[-\frac{i}{k_s r}\hat{r} + \phi\hat{\phi}\right].$$

where A_0, B_0, C_0 and D_0 are complex constants in general.

Observe inFigure-1, Figure-2 and Figure-3 that the approximations (13) and (15) are not valid near the origin and the negative real axis. In the particular case where $\Lambda = kr = x>1$ (positive real number), there is an agreement among functions as shown inFigure-4. In Figure-5 the behavior of $H_1^{(2)}(\Lambda)$, $iH_0^{(2)}(\Lambda)$ and $i\sqrt{2/\pi\Lambda}\,e^{i\pi/4}e^{-i\Lambda}$ along imaginary axis are also shown; here, the approximation is in agreement for $\Lambda = kr = iy < -i$ (negative imaginary number). This part is going to be useful afterwards.

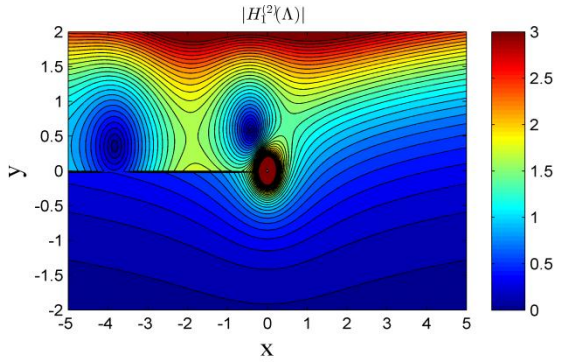

(a)

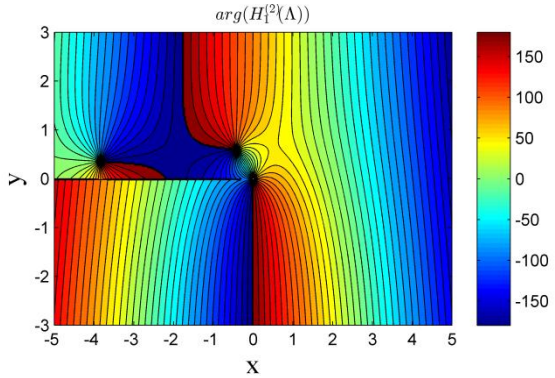

(b)

Figure-1. Contour maps of (a) modulus and (b) phase of the function $H_1^{(2)}(\Lambda)$. The argument $\Lambda = x + iy$ is a complex number.

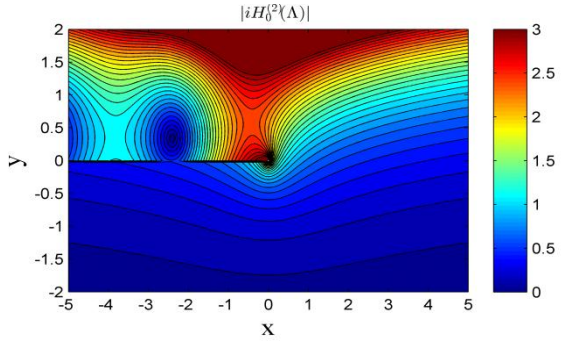

(a)

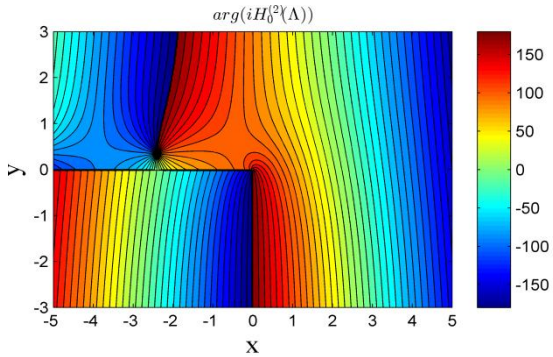

(b)

Figure-2. Contour maps of (a) modulus and (b) phase of the function $iH_0^{(2)}(\Lambda)$.

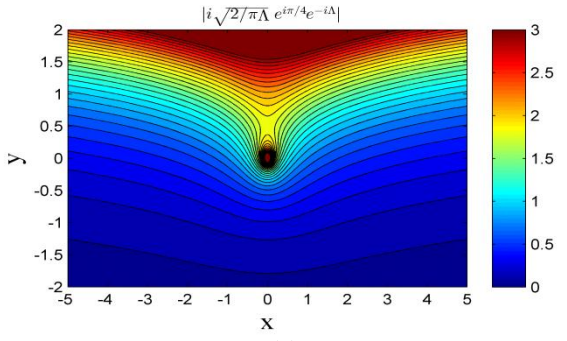

(a)

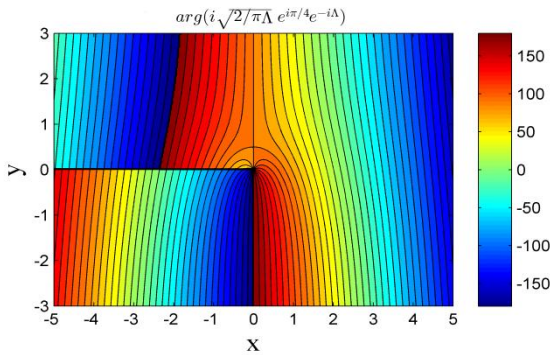

(b)

Figure-3. Contour maps of (a) modulus and (b) phase of the function $i\sqrt{2/\pi\Lambda}\, e^{i\pi/4}e^{-i\Lambda}$.

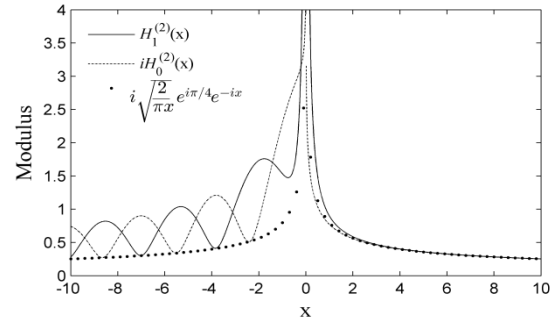

(a)

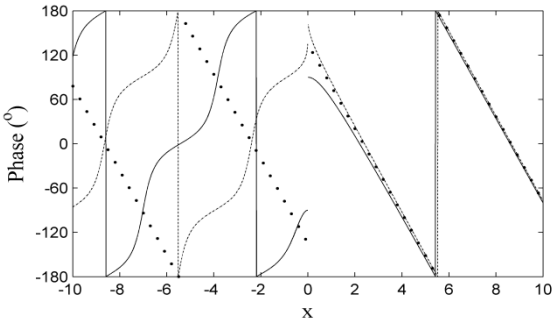

(b)

Figure-4. (a) Modulus and (b) phase of the functions $H_1^{(2)}(\Lambda)$, $iH_0^{(2)}(\Lambda)$ and $i\sqrt{2/\pi\Lambda}\, e^{i\pi/4}e^{-i\Lambda}$,where $\Lambda = x$ is a real argument.

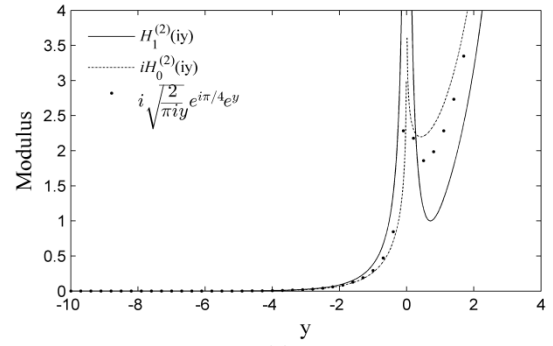

(a)

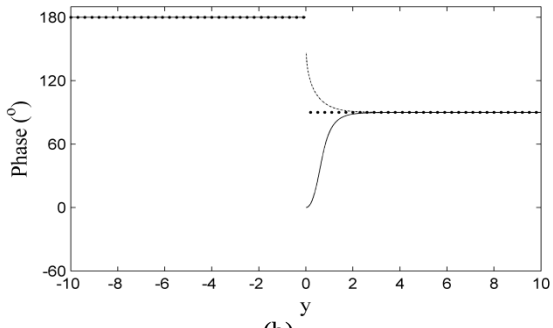

(b)

Figure-5. (a) Modulus and (b) phase of the functions $H_1^{(2)}(\Lambda)$, $iH_0^{(2)}(\Lambda)$ and $i\sqrt{2/\pi\Lambda}\, e^{i\pi/4}e^{-i\Lambda}$, where $\Lambda = iy$ is an imaginary argument.

Results in (12), (14) and (16) can be understood as body waves generated outward from line sources at $r = 0$. It can be seen that $\vec{u}_L^c$ is a homogeneous cylindrical wave with c_p propagation velocity that oscillates longitudinally (P or longitudinal wave); $\vec{u}_T^c$ is a homogeneous cylindrical wave with c_s propagation velocity that oscillates transversally (SV or transversal wave); $\vec{u}_p^{ce}$ is an inhomogeneous cylindrical wave with c_p propagation velocity, that oscillates elliptically; $\vec{u}_s^{ce}$ is an inhomogeneous cylindrical wave with c_s propagation velocity, that oscillates elliptically (see Figure-6).

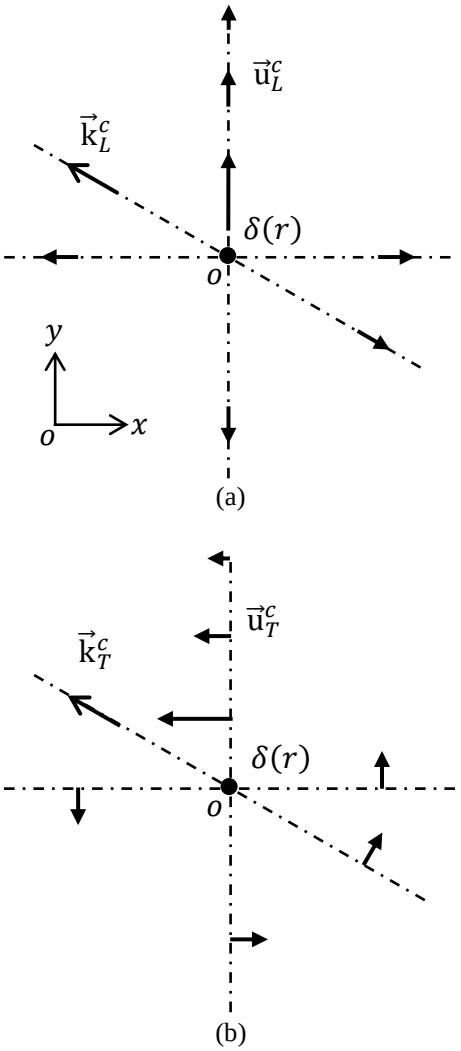

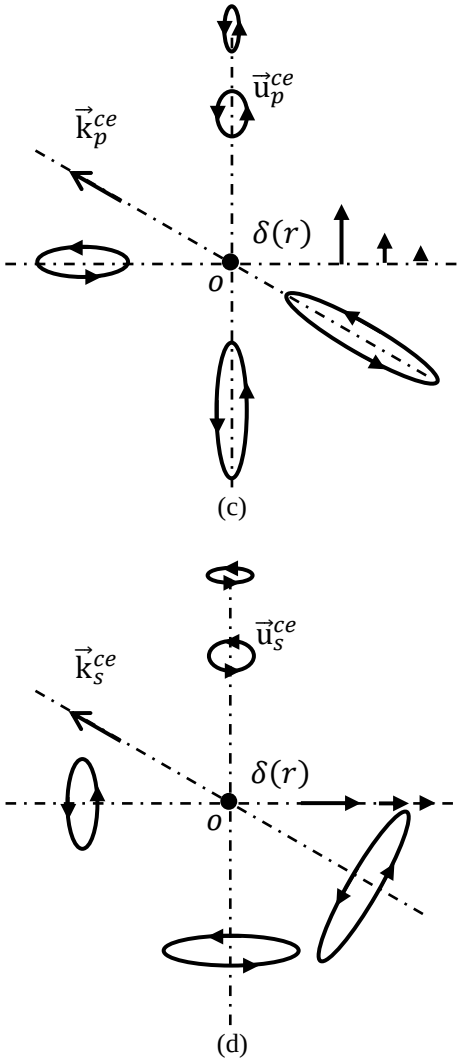

Figure-6. Diagrams of the displacement fields of (a) $\vec{u}_L^c$, (b) $\vec{u}_T^c$, (c) $\vec{u}_p^{ce}$, and (d) $\vec{u}_s^{ce}$ for $\nu = 2\pi$. The changes of displacement fields with ϕ and r are sketched in figure.

Note that when either $r \to \infty$ or $\phi \to 2\pi$, $\vec{u}_p^{ce}$ and $\vec{u}_s^{ce}$ tend to be longitudinal (L) and transversal (T) waves, respectively; but at $\phi = 0$, $\vec{u}_p^{ce}$ is transversal and $\vec{u}_s^{ce}$ is longitudinal, therefore, the radial component in $\vec{u}_p^{ce}$ and the azimuth in $\vec{u}_s^{ce}$ are not continuous, since their values are different at $\phi = 0$ and $\phi \to 2\pi$.

4.1. Particular cases: grazing longitudinal (*P*y) and transversal (*SV*y) waves of the Goodier-Bishop type

Here, the first approximation considers that ϕ is small, hence the arc longitude s tends to y, r tends to x; and the approximation for other parameters are shown in Figure-7.

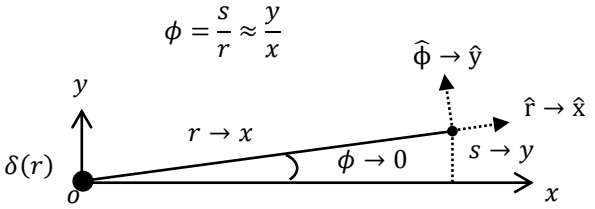

Figure-7. Approximations taken for waves in (16).

Returning to equation (16) and taking into account the previous approximations, it is obtained:

$$\begin{aligned}
\vec{u}_L^c &\approx \frac{B_0}{\sqrt{k_p x}} e^{-ik_p x}\hat{x}, \\
\vec{u}_T^c &\approx \frac{D_0}{\sqrt{k_s x}} e^{-ik_s x}\hat{y}, \\
\vec{u}_P^{ce} &\approx \frac{A_0}{(k_p x)^{3/2}} e^{-ik_p x}\left[k_p y\hat{x} + i\hat{y}\right], \\
\vec{u}_s^{ce} &\approx \frac{C_0}{(k_s x)^{3/2}} e^{-ik_s x}[-i\hat{x} + k_s y\hat{y}].
\end{aligned} \quad (17)$$

The second approach supposes that we are far away of the sources; therefore the amplitudes variation with respect to x is so slow that can be neglected in (17), obtaining finally:

$$\begin{aligned}
\vec{u}_L^c &\approx \vec{u}_L^{plane} = B_0 e^{-ik_p x}\hat{x}, \\
\vec{u}_T^c &\approx \vec{u}_T^{plane} = D_0 e^{-ik_s x}\hat{y}, \\
\vec{u}_P^{ce} &\approx \vec{u}_{Py} = A_0 e^{-ik_p x}\left[k_p y\hat{x} + i\hat{y}\right], \\
\vec{u}_s^{ce} &\approx \vec{u}_{SVy} = C_0 e^{-ik_s x}[-i\hat{x} + k_s y\hat{y}],
\end{aligned} \quad (18)$$

where $\vec{u}_L^{plane}$ and $\vec{u}_T^{plane}$ are typical longitudinal and transverse plane waves propagating in x direction. $\vec{u}_{Py}$ and $\vec{u}_{SVy}$ also propagate in x direction, but they have imaginary components and their amplitudes increase lineally with y. These kinds of waves are named *Py* and *SVy* by Goodier and Bishop [13]; and Graff [14] where the critical cases of grazing incidence of *P-SV* waves on a half-space are studied.

5. ANSÄTZE SOLUTIONS: PLANE SOURCES AND HOMOGENEOUS AND INHOMOGENEOUS WAVEFRONTS

Taking into mind the previous ideas, the authors propose the following potentials for primary (*P*) and secondary (*S*) waves (the ansätze or educated guess), for $0 \le \phi \le \nu$ and $r \ge 0$ with $0 \le \nu \le 2\pi$:

$$\begin{aligned}
\varphi^{pl} &= -\frac{1}{ik_p} H_0^{(2)}(\Lambda_p)[a\phi + b], \\
\vec{\psi}^{pl} &= \psi_z^{pl}\hat{z} = \frac{1}{ik_s} H_0^{(2)}(\Lambda_s)[c\phi + d]\hat{z},
\end{aligned} \quad (19)$$

being $\Lambda_p = k_p r\cos(\phi \pm \alpha_0)$ and $\Lambda_s = k_s r\cos(\phi \pm \beta_0)$, where a, b, c, d, α_0 and β_0 are complex constants in general; hence, the argument Λ of $H_0^{(2)}(\Lambda)$ can be complex.

One can show that the Laplacians of φ^{pl} and ψ_z^{pl} are (see Appendix 1)

$$\begin{aligned}
\nabla^2\varphi^{pl} - k_p^2[a\phi + b]\frac{d^2\left(-\frac{1}{ik_p}H_0^{(2)}(\Lambda_p)\right)}{d{\Lambda_p}^2} + \frac{2ak_p\sin\phi}{r}\frac{d\left(-\frac{1}{ik_p}H_0^{(2)}(\Lambda_p)\right)}{d\Lambda_p} &= \delta(\Lambda_p), \\
\nabla^2\psi_z^{pl} - k_s^2[c\phi + d]\frac{d^2\left(\frac{1}{ik_s}H_0^{(2)}(\Lambda_s)\right)}{d{\Lambda_s}^2} + \frac{2ck_s\sin\phi}{r}\frac{d\left(\frac{1}{ik_s}H_0^{(2)}(\Lambda_s)\right)}{d\Lambda_s} &= \delta(\Lambda_s);
\end{aligned} \quad (20)$$

observe that in $\Lambda_p = 0$ and $\Lambda_s = 0$, φ^{pl} and ψ_z^{pl} are singular. If it takes into account the approximation (13) in (11), it calculates

$$\frac{d^2H_0^{(2)}(\Lambda)}{d\Lambda^2} \approx -H_0^{(2)}(\Lambda),$$

which is valid for large Λ (in this validity range $\delta(\Lambda_p) = \delta(\Lambda_s) = 0$), and we replace in (20):

$$\begin{aligned}
\nabla^2\varphi^{pl} + k_p^2\varphi^{pl} + \frac{2ak_p\sin\phi}{k_p r}H_0^{(2)}(\Lambda_p) &\approx 0, \\
\nabla^2\psi_z^{pl} + k_s^2\psi_z^{pl} - \frac{2ck_s\sin\phi}{k_s r}H_0^{(2)}(\Lambda_s) &\approx 0;
\end{aligned}$$

the conditions in (3) are asymptotically achieved if kr is large (far-field: analysis far from the sources), obtaining finally

$$\begin{aligned}
\nabla^2\varphi^{pl} + k_p^2\varphi^{pl} &\approx 0, \\
\nabla^2\psi_z^{pl} + k_s^2\psi_z^{pl} &\approx 0, \\
\nabla\cdot\vec{\psi}^{pl} &= 0.
\end{aligned} \quad (21)$$

It is worth noting that φ^{pl} and ψ_z^{pl} in (19) are singular in $\Lambda_p = 0$ and $\Lambda_s = 0$, thus, this generates Dirac delta functions in (20) that represent sources, but these function can represent, in fact, elastic wave in far-field due to that satisfy asymptotically the equations in (3) (or (21)) far from the sources. Based on these ideas, we are going to show the generation of elastic wave in far-field from the sources in the next section, together to the study of the particular cases of the Hankel function argument.

5.1. Particular cases

5.1.1. Homogeneous and inhomogeneous plane wavefronts

First, when the argument Λ is real is analyzed. Based on Figure-4 and in previous section, the

approximations (13) and (21) are taken as valid for positive real argument and far the origin, that is, when $\Lambda_p \gg 0$ and $\Lambda_s \gg 0$. This implies that must be taken $|\Lambda_p| = k_p r|\cos(\phi \pm \alpha_0)| \equiv \Lambda_p^{\pm\alpha_0}$ and $|\Lambda_s| = k_s r|\cos(\phi \pm \beta_0)| \equiv \Lambda_s^{\pm\beta_0}$ to cover all space far from the sources.

Note that when Λ_p and Λ_s are real, φ^{pl} is singular in $r = 0$, $\phi = \frac{\pi}{2} \mp \alpha_0$ and $\phi = \frac{3\pi}{2} \mp \alpha_0$; and ψ_z^{pl} is singular in $r = 0$, $\phi = \frac{\pi}{2} \mp \beta_0$ and $\phi = \frac{3\pi}{2} \mp \beta_0$, where $|\Lambda_p| = |\Lambda_s| = 0$. Then, the Dirac delta functions in (20), for $\nu = 2\pi$, can be written as:

$$\delta(|\Lambda_p|) = \left\{\frac{\delta(r)}{r} + \delta\left(\phi - \left(\frac{\pi}{2} \mp \alpha_0\right)\right) + \delta\left(\phi - \left(\frac{3\pi}{2} \mp \alpha_0\right)\right)\right\} \equiv \delta\left(\Lambda_p^{\pm\alpha_0}\right),$$
$$\delta(|\Lambda_s|) = \left\{\frac{\delta(r)}{r} + \delta\left(\phi - \left(\frac{\pi}{2} \mp \beta_0\right)\right) + \delta\left(\phi - \left(\frac{3\pi}{2} \mp \beta_0\right)\right)\right\} \equiv \delta\left(\Lambda_s^{\pm\beta_0}\right),$$

which represent plane sources such as are shown in Figure-8, where the *S*case (*SV*or transversal wave) is sketched with positive real argument $\Lambda_s = k_s r|\cos(\phi \pm \beta_0)|$.

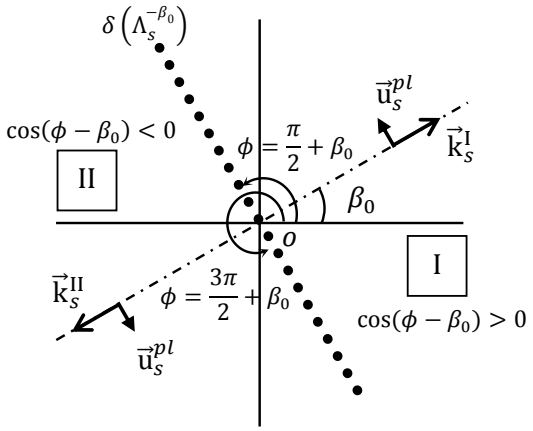

(a)

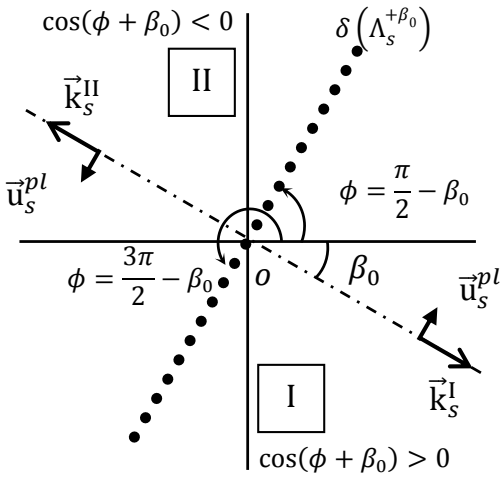

(b)

Figure-8. Diagrams in far-field of the displacement field $\vec{u}_s^{pl}$ generated by plane sources. The two regions defined by plane sources also are shown in figures and described in (22).

In view of Figure-8, the following regions are defined:

$$\text{Region I-}S = \begin{cases} \beta_0 - \frac{\pi}{2} < \phi < \beta_0 + \frac{\pi}{2}, \text{for } \cos(\phi - \beta_0) \\ -\frac{\pi}{2} - \beta_0 < \phi < \frac{\pi}{2} - \beta_0, \text{for } \cos(\phi + \beta_0) \end{cases}$$
$$\text{Region II-}S = \begin{cases} \beta_0 + \frac{\pi}{2} < \phi < \beta_0 + \frac{3\pi}{2}, \text{for } \cos(\phi - \beta_0) \\ \frac{\pi}{2} - \beta_0 < \phi < \frac{3\pi}{2} - \beta_0, \text{for } \cos(\phi + \beta_0) \end{cases} \quad (22)$$

Likewise, it can be defined for *P* case:

$$\text{Region I-}P = \begin{cases} \alpha_0 - \frac{\pi}{2} < \phi < \alpha_0 + \frac{\pi}{2}, \text{for } \cos(\phi - \alpha_0) \\ -\frac{\pi}{2} - \alpha_0 < \phi < \frac{\pi}{2} - \alpha_0, \text{for } \cos(\phi + \alpha_0) \end{cases}$$
$$\text{Region II-}P = \begin{cases} \alpha_0 + \frac{\pi}{2} < \phi < \alpha_0 + \frac{3\pi}{2}, \text{for } \cos(\phi - \alpha_0) \\ \frac{\pi}{2} - \alpha_0 < \phi < \frac{3\pi}{2} - \alpha_0, \text{for } \cos(\phi + \alpha_0) \end{cases} \quad (23)$$

Also from Figure-8, it can be observed that for the case of this subsection

$$|\Lambda_s| = \left\{\begin{array}{l} \vec{k}_s^{I} \cdot \vec{r} = k_s r \cos(\phi \pm \beta_0) \text{ in region I-}S \\ \vec{k}_s^{II} \cdot \vec{r} = -k_s r \cos(\phi \pm \beta_0) \text{ in region II-}S \end{array}\right\} \equiv k_s r \cos(\phi \pm \beta_0)\, \text{sgn}(\cos(\phi \pm \beta_0)), \quad (24)$$

$$\frac{\partial|\cos(\phi \pm \beta_0)|}{\partial\phi} = \left\{\begin{array}{l} -\sin(\phi \pm \beta_0) \text{ in region I-}S \\ \sin(\phi \pm \beta_0) \text{ in region II-}S \end{array}\right\} \equiv -\sin(\phi \pm \beta_0)\, \text{sgn}(\cos(\phi \pm \beta_0)),$$

where $\mathrm{sgn}(\eta)$ is the Sign Function and is defined as

$$\mathrm{sgn}(\cos(\phi \pm \beta_0)) = \begin{cases} 1, \text{ in region I-}SV \\ -1, \text{ in region II-}SV \end{cases}.$$

Now, the fields *P-S*are derived bytaking into account (19), (13) and (24) in equation (2), it is obtained that

$$\vec{u}_P^{pl} = \nabla\varphi^{pl} \approx b\vec{u}_L^{pl} + a\vec{u}_p^{ple} = \vec{u}_L^{pl}\,[a\phi + b] + \frac{ai}{k_p r}H_0^{(2)}(|\Lambda_p|)\hat{\phi}$$
$$\vec{u}_s^{pl} = \nabla \times \vec{\psi}^{pl} \approx d\vec{u}_T^{pl} + c\vec{u}_s^{ple} = \vec{u}_T^{pl}\,[c\phi + d] - \frac{ci}{k_s r}H_0^{(2)}(|\Lambda_s|)\hat{\phi}, \quad (25)$$

where

$$\vec{u}_L^{pl} \approx H_0^{(2)}(|\Lambda_p|)\left[|\cos(\phi \pm \alpha_0)|\hat{r} - \mathrm{sgn}(\cos(\phi \pm \alpha_0))\sin(\phi \pm \alpha_0)\,\hat{\phi}\right],$$

$$\vec{u}_T^{pl} \approx H_0^{(2)}(|\Lambda_s|)\left[\mathrm{sgn}(\cos(\phi \pm \beta_0))\sin(\phi \pm \beta_0)\,\hat{r} + |\cos(\phi \pm \beta_0)|\hat{\phi}\right],$$

$$\vec{u}_P^{ple} \approx \phi\vec{u}_L^{pl} + \frac{i}{k_p r}H_0^{(2)}(|\Lambda_p|)\hat{\phi}$$
$$\vec{u}_s^{ple} \approx \phi\vec{u}_T^{pl} - \frac{i}{k_s r}H_0^{(2)}(|\Lambda_s|)\hat{r}, \quad (26)$$

If it is taking into account the asymptotic expansion (15), it is achieved:

$$\vec{u}_L^{pl} \approx \frac{1}{\sqrt{|\Lambda_p|}}e^{-i|\Lambda_p|}\left[|\cos(\phi \pm \alpha_0)|\hat{r} - \mathrm{sgn}(\cos(\phi \pm \alpha_0))\sin(\phi \pm \alpha_0)\,\hat{\phi}\right],$$

$$\vec{u}_T^{pl} \approx \frac{1}{\sqrt{|\Lambda_s|}}e^{-i|\Lambda_s|}\left[\mathrm{sgn}(\cos(\phi \pm \beta_0))\sin(\phi \pm \beta_0)\,\hat{r} + |\cos(\phi \pm \beta_0)|\hat{\phi}\right],$$

$$\vec{u}_P^{ple} \approx \phi\vec{u}_L^{pl} + \frac{i}{k_p r\sqrt{|\Lambda_p|}}e^{-i|\Lambda_p|}\hat{\phi}$$
$$\vec{u}_s^{ple} \approx \phi\vec{u}_T^{pl} - \frac{i}{k_s r\sqrt{|\Lambda_s|}}e^{-i|\Lambda_s|}\hat{r}, \quad (27)$$

Results in (26) and (27) can be interpreted as body waves (in far-field) generated outward from plane sources. It can be seen that $\vec{u}_L^{pl}$ is a homogeneous plane wave with c_p propagation velocity that oscillates longitudinally (*P* or longitudinal wave); $\vec{u}_T^{pl}$ is a homogeneous plane wave with c_s propagation velocity that oscillates transversally (*SV* or transversal wave); $\vec{u}_p^{ple}$ is an inhomogeneous plane wave with c_p propagation velocity, that oscillates elliptically; $\vec{u}_s^{ple}$ is an inhomogeneous plane wave with c_s propagation velocity, that oscillates elliptically (see Figure-9). Note also that the decaying of amplitudes is given when we move away from the plane sources.

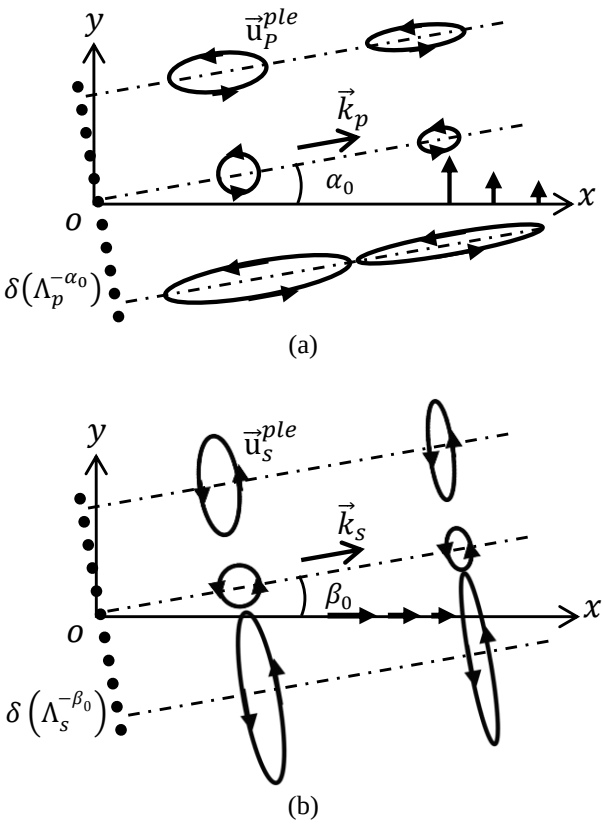

Figure-9. Diagrams in far-fieldof the displacement fields of (a) $\vec{u}_p^{ple}$ and (b) $\vec{u}_s^{ple}$ for $\nu = 2\pi$. The changes of displacement fields with ϕ and r are shown in figures.

It is also important to note here that when either $r \to \infty$ or $\phi \to 2\pi$, $\vec{u}_p^{ple}$ and $\vec{u}_s^{ple}$ tend to be longitudinal (*L*) and transversal (*T*) waves, respectively; but at $\phi = 0$, $\vec{u}_p^{ple}$ is transversal and $\vec{u}_s^{ple}$ is longitudinal, therefore, they are not continuous, since their values are different at $\phi = 0$ and $\phi = 2\pi$.

5.1.2. Homogeneous plane wave fronts

Another approximation that can be taken is to suppose that we are far away of the plane sources, therefore the amplitudes change so slowly with respect to $|\Lambda_p|$ and $|\Lambda_s|$, thus, they can be taken constants and the terms $\propto 1/kr\sqrt{|\Lambda|}$ are neglected in (27). Here, the regions I with $\cos(\phi - \alpha_0) > 0$ is taken; obtaining finally the typical homogeneous plane waves in (28) that are illustrated in Figure-10.

$$\begin{aligned}\vec{u}_L^{pl} &\approx e^{-ik_p r\cos(\phi-\alpha_0)}\left[\cos(\phi-\alpha_0)\,\hat{r}-\sin(\phi-\alpha_0)\,\hat{\phi}\right],\\ \vec{u}_T^{pl} &\approx e^{-ik_s r\cos(\phi-\beta_0)}\left[\sin(\phi-\beta_0)\,\hat{r}+\cos(\phi-\beta_0)\,\hat{\phi}\right],\\ \vec{u}_P^{ple} &\approx \phi\vec{u}_L^{pl},\\ \vec{u}_s^{ple} &\approx \phi\vec{u}_T^{pl}.\end{aligned} \quad (28)$$

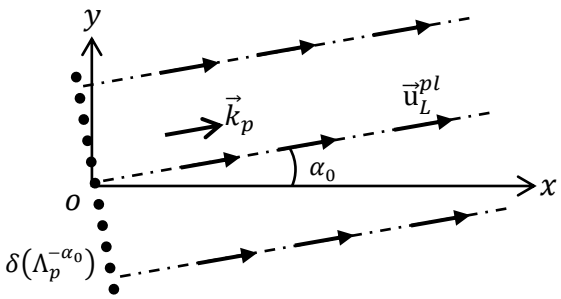

(a)

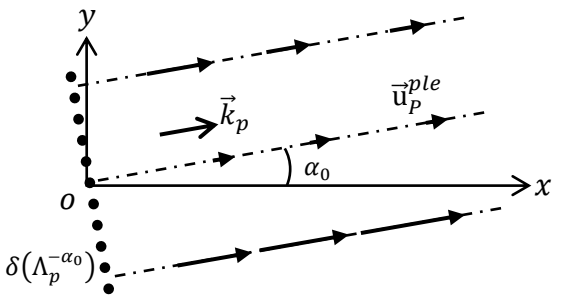

(b)

Figure-10. Diagrams in far-fieldof the displacement fields of (a) $\vec{u}_L^{pl}$ and (b) $\vec{u}_T^{pl}$. The changes of displacement fields with ϕ and r are shown in figures.

5.1.3. Grazing longitudinal (*P*y) and transversal (*SV*y) waves of the Goodier-Bishop type

First, it is taken $\alpha_0 = 0$ and $\beta_0 = 0$. Second, in the same manner as in the section 4.1, it is considered that ϕ is small, hence $\cos(\phi) \to 1$, $\sin(\phi) \to 0$, $s \to y$, $r \to x$, $\phi = s/r \approx y/x$, $\hat{\phi} \to \hat{y}$ and $\hat{r} \to \hat{x}$ (see Figure-7). Now, returning to equation (27) and taking into account the previous approximations, it is obtained that

$$\begin{aligned}\vec{u}_L^{pl} &\approx \frac{1}{\sqrt{k_p x}}e^{-ik_p x}\hat{x},\\ \vec{u}_T^{pl} &\approx \frac{1}{\sqrt{k_s x}}e^{-ik_s x}\hat{y},\\ \vec{u}_P^{ple} &\approx \frac{1}{(k_p x)^{3/2}}e^{-ik_p x}\left[k_p y\hat{x}+i\hat{y}\right],\\ \vec{u}_s^{ple} &\approx \frac{1}{(k_s x)^{3/2}}e^{-ik_s x}\left[-i\hat{x}+k_s y\hat{y}\right].\end{aligned} \quad (29)$$

Finally, it is supposed that we are far away of the sources; therefore, the amplitudes variation with respect to x is so slow that can be neglected in (29), thus obtaining the same result in (18): $\vec{u}_L^{pl} \approx \vec{u}_L^{plane}$, $\vec{u}_T^{pl} \approx \vec{u}_T^{plane}$, $\vec{u}_P^{ple} \approx \vec{u}_{Py}$, $\vec{u}_s^{ple} \approx \vec{u}_{SVy}$.

5.1.4. Surface *P* wave

Now, the case when Λ is complex is analyzed. Here, the expressions $\vec{u}_L^{pl}$ and $\vec{u}_p^{ple}$ from (26) for region I defined in (23) are worked and shown in Figure-12 (see also Figure-8 for identifying the region I):

$$\vec{u}_L^{pl} = H_0^{(2)}(\Lambda_p)\left[\cos(\phi+\alpha_0)\,\hat{r}-\sin(\phi+\alpha_0)\,\hat{\phi}\right],$$

$$\vec{u}_P^{ple} = \phi\vec{u}_L^{pl} + \frac{i}{k_p r}H_0^{(2)}(\Lambda_p)\hat{\phi}.$$

Then, if an imaginary angle $\alpha_0 = i\gamma_0$ is taken, with γ_0 positive real:

$$\begin{aligned}\vec{u}_L^{pl} &= H_0^{(2)}(\Lambda_p^{+i\gamma_0})\left[\cos(\phi+i\gamma_0)\,\hat{r}-\sin(\phi+i\gamma_0)\,\hat{\phi}\right],\\ \vec{u}_P^{ple} &= \phi\vec{u}_L^{pl} + \frac{i}{k_p r}H_0^{(2)}(\Lambda_p^{+i\gamma_0})\hat{\phi},\end{aligned} \quad (30)$$

where $\Lambda_p^{+i\gamma_0} = k_p r\cos(\phi+i\gamma_0)$. Considering the following relations:

$$\begin{aligned}\sin(\phi\pm i\gamma_0) &= \sin\phi\cosh\gamma_0 \pm i\cos\phi\sinh\gamma_0,\\ \cos(\phi\pm i\gamma_0) &= \cos\phi\cosh\gamma_0 \mp i\sin\phi\sinh\gamma_0;\end{aligned} \quad (31)$$

and transforming from Cylindrical to Cartesian system, it is obtained:

$$\vec{u}_L^{pl} = H_0^{(2)}(\Lambda_p^{+i\gamma_0})[\cosh\gamma_0\,\hat{x}-i\sinh\gamma_0\,\hat{y}], \quad (32)$$

$$\vec{u}_P^{ple} = \tan^{-1}\left(\frac{y}{x}\right)\vec{u}_L^{pl} + \frac{i}{k_p\sqrt{x^2+y^2}}H_0^{(2)}(\Lambda_p^{+i\gamma_0})\left[-\frac{y}{\sqrt{x^2+y^2}}\hat{x}+\frac{x}{\sqrt{x^2+y^2}}\hat{y}\right],$$

where $\Lambda_p^{+i\gamma_0} = k_p x\cosh\gamma_0 - ik_p y\sinh\gamma_0$. Note that $x \geq 0$ and $y \geq 0$ for the problems shown in Figure-11 and Figure-12. Here can also be observed that the argument $\Lambda_p^{+i\gamma_0} = \mathrm{x} + i\mathrm{y} = k_p x\cosh\gamma_0 - ik_p y\sinh\gamma_0$ (for $x > 0$ and $y > 0$, then, $\mathrm{x} > 0$ and $\mathrm{y} < 0$) move into the validity range of approximations that are shown in

section 4 (see Figure-1, 2, 3, 4 and 5), in other words, we move in the fourth quadrant of the complex plane ($x > 0$ and $y < 0$) to cover the half-space that is shown in Figure-12.

Then, the Dirac delta functions in (20), for $\nu = 2\pi$, can be written for this case as:

$$\delta\left(\Lambda_p^{+i\gamma_0}\right) = \frac{\delta(r)}{r} + \delta\left(\phi - \left(\frac{\pi}{2} - i\gamma_0\right)\right) + \delta\left(\phi - \left(\frac{3\pi}{2} - i\gamma_0\right)\right) = \frac{\delta(r)}{r}, \quad (33)$$

due to that $H_0^{(2)}\left(\Lambda_p^{+i\gamma_0}\right)$ (or φ^{pl} in equations (19)) is singular when $\Lambda_p^{+i\gamma_0} = k_p r\cos(\phi + i\gamma_0)$ $= k_p x\cosh\gamma_0 - ik_p y\sinh\gamma_0 = 0$, and it can be observed that $\Lambda_p^{+i\gamma_0}$ is zero in $r = 0$ or $x = 0$ and $y = 0$ simultaneously. From another point of view, as ϕ is always real, then $\delta\left(\phi - \left(\frac{\pi}{2} - i\gamma_0\right)\right)$ and $\delta\left(\phi - \left(\frac{3\pi}{2} - i\gamma_0\right)\right)$ are always zero, unless $\phi = \frac{\pi}{2} - i\gamma_0$ and $\phi = \frac{3\pi}{2} - i\gamma_0$, who could be interpreted as imaginary plane sources, such as shown in Figure-13. Therefore, there are line sources instead plane sources when ? is real (see Figure-12).

Afterward, taking the asymptotic expansion (15) in (30):

$$\vec{u}_L^{pl} \approx \frac{1}{\sqrt{\Lambda_p^{+i\gamma_0}}} e^{-i\Lambda_p^{+i\gamma_0}}\left[\cos(\phi + i\gamma_0)\,\hat{r} - \sin(\phi + i\gamma_0)\,\hat{\phi}\right], \quad (34)$$

$$\vec{u}_P^{ple} \approx \phi\vec{u}_L^{pl} + \frac{i}{k_p r\sqrt{\Lambda_p^{+i\gamma_0}}} e^{-i\Lambda_p^{+i\gamma_0}}\hat{\phi} \approx \frac{e^{-i\Lambda_p^{+i\gamma_0}}}{k_p r\sqrt{\Lambda_p^{+i\gamma_0}}}\left\{k_p r\phi\left[\cos(\phi + i\gamma_0)\,\hat{r} - \sin(\phi + i\gamma_0)\,\hat{\phi}\right] + i\hat{\phi}\right\}$$

Note that in (34), the amplitude decays from source. Now it is supposed to be far away of the source, hence, the amplitude variation with respect to $\Lambda_p^{+i\gamma_0}$ is very slow and it can be neglected, obtaining finally:

$$\vec{u}_L^{pl} \approx e^{-i\Lambda_p^{+i\gamma_0}}\left[\cos(\phi + i\gamma_0)\,\hat{r} - \sin(\phi + i\gamma_0)\,\hat{\phi}\right]$$
$$\approx e^{-y k_p \sinh\gamma_0} e^{-ix k_{psurf}}\left[\cosh\gamma_0\,\hat{x} - i\sinh\gamma_0\,\hat{y}\right], \quad (35)$$

$$\vec{u}_P^{ple} \approx e^{-i\Lambda_p^{+i\gamma_0}}\left\{k_p r\phi\left[\cos(\phi + i\gamma_0)\,\hat{r} - \sin(\phi + i\gamma_0)\,\hat{\phi}\right] + i\hat{\phi}\right\}.$$

where $k_{psurf} = k_p\cosh\gamma_0 = \omega/c_{psurf} = \omega\cosh\gamma_0/c_p$ with $c_{psurf} = c_p/\cosh\gamma_0$. $\vec{u}_L^{pl}$ in (35) is atypical surface *P* waves ($\vec{u}_p^{Ref} = b\vec{u}_L^{pl}$ in Figure-11(b), where b is the amplitude) that travels with c_{psurf} velocity and emerges in the reflection process of a homogeneous plane *SV* wave falling on a half-space ($\vec{u}_{sv}^{inc}$ in Figure-11) below the incidence critical angle β_{cr}, as is shown by Graff [14] and Anchenbach [11], that for case of the Figure-11(b) is obtained:

$$\begin{aligned}\sin i\gamma_0 &= i\sinh\gamma_0 \\ &= i\sqrt{K^2\cos^2\beta_{inc} - 1} \\ &= iK\sqrt{\cos^2\beta_{inc} - K^{-2}},\end{aligned} \quad (36)$$

$$\cos i\gamma_0 = \cosh\gamma_0 = K\cos\beta_{inc},$$

$$c_{psurf} = c_s/\cos\beta_{inc} = c_p/\cosh\gamma_0,$$

with $K = k_s/k_p = c_p/c_s$.

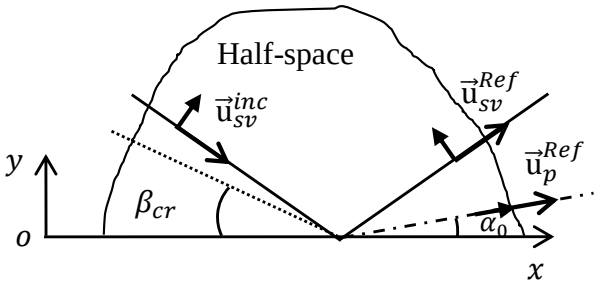

(a)

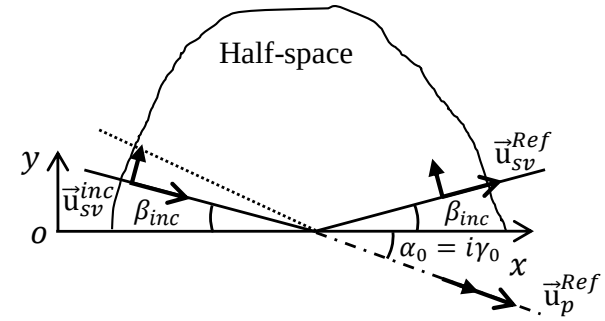

(b)

Figure-11. Reflection of an incident plane *SV* wave on a half-space: (a) Falling above and (b) below the incidence critical angle. In (b) is shown the generation of an inhomogeneous *P*wave (surface *P* wave), with an imaginary angle, from a "Geometrical" point of view.

Finally, considering the approximations given in section 4.1, it is obtained that

$$\vec{u}_p^{ple} \approx e^{-y k_p \sinh\gamma_0} e^{-ix k_{psurf}}\left\{k_p y\left[\cosh\gamma_0\,\hat{x} + i\left(\frac{1}{k_p y} - \sinh\gamma_0\right)\hat{y}\right]\right\} \quad (37)$$

where if $\gamma_0 = 0$ the Goodier-Bishop wave, $\vec{u}_{Py}$ in (18), is achieved.

In this section we have shown that (30), in fact, are surface *P* waves and in the case of the Figure-11(b) that $\gamma_0 = \cosh^{-1}\left(\frac{c_p}{c_s}\cos\beta_0\right)$, where $\frac{c_p}{c_s}\cos\beta_0 > 1$. In

Figure-12 the "Geometrical" and "physical" point of view of the inhomogeneous waves in (34) are shown.

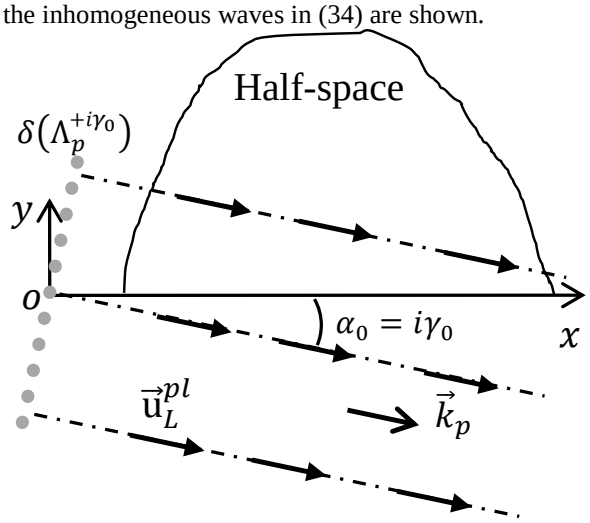

(a)

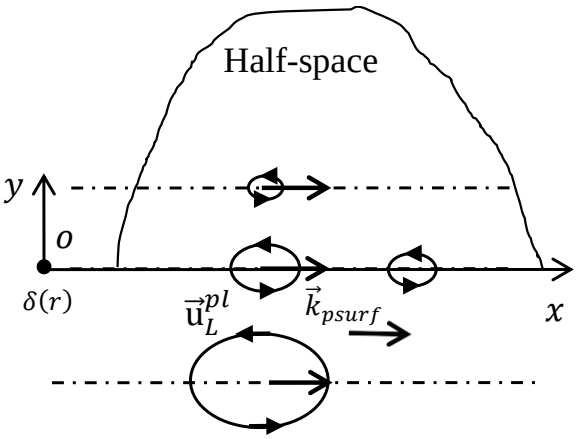

(b)

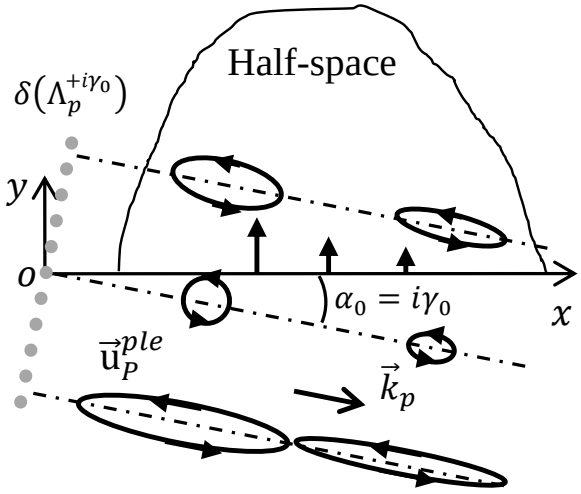

(c)

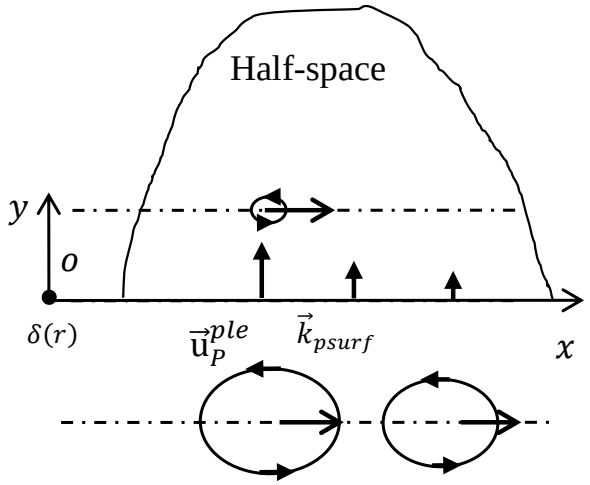

(d)

Figure-12. Diagrams in far-field of surface *P* waves for the half-space from: (a) and (c)a "Geometrical" point of view, (b) and (d)a "Physical" point of view. Plane sources (gray points) in (a) and (c) are imagined and we have drawn it to try to visualize, from a geometrical point of view, the origination of the inhomogeneous plane waves emerging with imaginary angles, since the one real source is a lineat the origin.

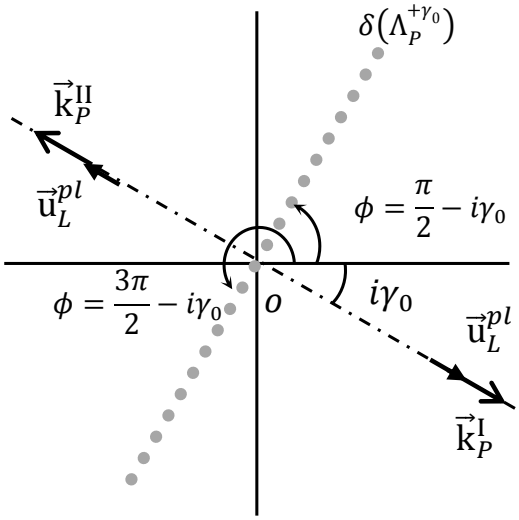

Figure-13. Diagrams in far-field of the displacement field $\vec{u}_L^{pl}$ generated by imaginary plane sources (gray points).

5.1.5 Rayleigh surface wave

In order to illustrate, the expressions in (26) for region I defined in (22) and (23) are worked and shown in Figure-14(a) (see also Figure-8 for identifying the region I):

$$\vec{u}_L^{pl} = H_0^{(2)}(\Lambda_p)\left[\cos(\phi + \alpha_0)\,\hat{r} - \sin(\phi + \alpha_0)\,\hat{\phi}\right],$$

$$\vec{u}_T^{pl} = H_0^{(2)}(\Lambda_s)\left[\sin(\phi + \beta_0)\,\hat{r} + \cos(\phi + \beta_0)\,\hat{\phi}\right],$$

$$\vec{u}_P^{ple} = \phi\vec{u}_L^{pl} + \frac{i}{k_p r}H_0^{(2)}(\Lambda_p)\hat{\phi},$$

$$\vec{u}_s^{ple} = \phi\vec{u}_T^{pl} - \frac{i}{k_s r}H_0^{(2)}(\Lambda_s)\hat{r}.$$

Then, if imaginary angles $\alpha_0 = i\gamma_0$ and $\beta_0 = i\theta_0$ are taken, being γ_0 and θ_0 positive real numbers:

$$\vec{u}_L^{pl} = H_0^{(2)}(\Lambda_p^{+i\gamma_0})\left[\cos(\phi + i\gamma_0)\,\hat{r} - \sin(\phi + i\gamma_0)\,\hat{\phi}\right],$$

$$\vec{u}_T^{pl} = H_0^{(2)}(\Lambda_s^{+i\theta_0})\left[\sin(\phi + i\theta_0)\,\hat{r} + \cos(\phi + i\theta_0)\,\hat{\phi}\right],$$

$$\begin{aligned}\vec{u}_P^{ple} &= \phi\vec{u}_L^{pl} + \frac{i}{k_p r}H_0^{(2)}(\Lambda_p^{+i\gamma_0})\hat{\phi},\\ \vec{u}_s^{ple} &= \phi\vec{u}_T^{pl} - \frac{i}{k_s r}H_0^{(2)}(\Lambda_s^{+i\theta_0})\hat{r}.\end{aligned} \quad (38)$$

where $\Lambda_p^{+i\gamma_0} = k_p r\cos(\phi + i\gamma_0)$ and $\Lambda_s^{+i\theta_0} = k_s r\cos(\phi + i\theta_0)$. Considering the relations (31) and changing from cylindrical system to Cartesian system, it is obtained:

$$\vec{u}_L^{pl} = H_0^{(2)}(\Lambda_p^{+i\gamma_0})[\cosh\gamma_0\,\hat{x} - i\sinh\gamma_0\,\hat{y}],$$

$$\vec{u}_T^{pl} = H_0^{(2)}(\Lambda_s^{+i\theta_0})[i\sinh\theta_0\,\hat{x} + \cosh\theta_0\,\hat{y}], \quad (39)$$

$$\vec{u}_P^{ple} = \tan^{-1}\left(\frac{y}{x}\right)\vec{u}_L^{pl} + \frac{i}{k_p\sqrt{x^2+y^2}}H_0^{(2)}(\Lambda_p^{+i\gamma_0})\left[-\frac{y}{\sqrt{x^2+y^2}}\hat{x} + \frac{x}{\sqrt{x^2+y^2}}\hat{y}\right]$$

$$\vec{u}_s^{ple} = \tan^{-1}\left(\frac{y}{x}\right)\vec{u}_T^{pl} - \frac{i}{k_s\sqrt{x^2+y^2}}H_0^{(2)}(\Lambda_s^{+i\theta_0})\left[\frac{x}{\sqrt{x^2+y^2}}\hat{x} + \frac{y}{\sqrt{x^2+y^2}}\hat{y}\right]$$

where $\Lambda_p^{+i\gamma_0} = k_p x\cosh\gamma_0 - ik_p y\sinh\gamma_0$ and $\Lambda_s^{+i\theta_0} = k_s x\cosh\theta_0 - ik_s y\sinh\theta_0$. Note that $x \geq 0$ and $y \geq 0$ for the problem shown in Figure-14. Here can also be observed that the arguments $\Lambda_p^{+i\gamma_0}$ and $\Lambda_s^{+i\theta_0}$, as in the previous subsection, move into the validity range of approximations that are shown in section 4.

Then, Dirac delta functions in (20) for this case, the same as in the previous subsection, are given by

$$\delta(\Lambda_p^{+i\gamma_0}) = \delta(\Lambda_s^{+i\theta_0}) = \frac{\delta(r)}{r}, \quad (40)$$

here also there are line sources instead plane sources when Λ is real (see Figure-14). Taking into account the approximation (15) in (38), it is obtained:

$$\vec{u}_L^{pl} \approx \frac{1}{\sqrt{\Lambda_p^{+i\gamma_0}}}e^{-i\Lambda_p^{+i\gamma_0}}\left[\cos(\phi + i\gamma_0)\,\hat{r} - \sin(\phi + i\gamma_0)\,\hat{\phi}\right],$$

$$\vec{u}_T^{pl} \approx \frac{1}{\sqrt{\Lambda_s^{+i\theta_0}}}e^{-i\Lambda_s^{+i\theta_0}}\left[\sin(\phi + i\theta_0)\,\hat{r} + \cos(\phi + i\theta_0)\,\hat{\phi}\right],$$

$$\begin{aligned}\vec{u}_P^{ple} &\approx \phi\vec{u}_L^{pl} + \frac{i}{k_p r\sqrt{\Lambda_p^{+i\gamma_0}}}e^{-i\Lambda_p^{+i\gamma_0}}\hat{\phi}\\ &\approx \frac{e^{-i\Lambda_p^{+i\gamma_0}}}{k_p r\sqrt{\Lambda_p^{+i\gamma_0}}}\{k_p r\phi\left[\cos(\phi + i\gamma_0)\,\hat{r} - \sin(\phi + i\gamma_0)\,\hat{\phi}\right] + i\hat{\phi}\},\end{aligned} \quad (41)$$

$$\begin{aligned}\vec{u}_s^{ple} &\approx \phi\vec{u}_T^{pl} - \frac{i}{k_s r\sqrt{\Lambda_s^{+i\theta_0}}}e^{-i\Lambda_s^{+i\theta_0}}\hat{r}\\ &\approx \frac{e^{-i\Lambda_s^{+i\theta_0}}}{k_s r\sqrt{\Lambda_s^{+i\theta_0}}}\{k_s r\phi\left[\sin(\phi + i\theta_0)\,\hat{r} + \cos(\phi + i\theta_0)\,\hat{\phi}\right] - i\hat{r}\}.\end{aligned}$$

Note also that in (41), the amplitude decays from sources. Finally, it is supposed to be far away from the sources, hence, the amplitude variation with respect to Λ is very slow and it can be neglected, obtaining finally:

$$\begin{aligned}\vec{u}_L^{pl} &\approx e^{-i\Lambda_p^{+i\gamma_0}}\left[\cos(\phi + i\gamma_0)\,\hat{r} - \sin(\phi + i\gamma_0)\,\hat{\phi}\right]\\ &\approx e^{-yk_p\sinh\gamma_0}e^{-ixk_{psurf}}\left[\cosh\gamma_0\,\hat{x} - i\sinh\gamma_0\,\hat{y}\right],\\ \vec{u}_T^{pl} &\approx e^{-i\Lambda_s^{+i\theta_0}}\left[\sin(\phi + i\theta_0)\,\hat{r} + \cos(\phi + i\theta_0)\,\hat{\phi}\right]\\ &\approx e^{-yk_s\sinh\theta_0}e^{-ixk_{ssurf}}\left[i\sinh\theta_0\,\hat{x} + \cosh\theta_0\,\hat{y}\right],\\ \vec{u}_P^{ple} &\approx e^{-i\Lambda_p^{+i\gamma_0}}\{k_p r\phi\left[\cos(\phi + i\gamma_0)\,\hat{r} - \sin(\phi + i\gamma_0)\,\hat{\phi}\right] + i\hat{\phi}\},\\ \vec{u}_s^{ple} &\approx e^{-i\Lambda_s^{+i\theta_0}}\{k_s r\phi\left[\sin(\phi + i\theta_0)\,\hat{r} + \cos(\phi + i\theta_0)\,\hat{\phi}\right] - i\hat{r}\}.\end{aligned} \quad (42)$$

where $k_{psurf} = k_p\cosh\gamma_0 = \omega/c_{psurf} = \omega\cosh\gamma_0/c_p$ and $k_{ssurf} = k_s\cosh\theta_0 = \omega/c_{ssurf} = \omega\cosh\theta_0/c_s$ with $c_{psurf} = c_p/\cosh\gamma_0$ and $c_{ssurf} = c_s/\cosh\theta_0$. Expressions in (42) are *P* and *S* surface waves that travel at velocities c_{psurf} and c_{ssurf}, respectively. Then, it is obtained that

$$\cosh\gamma_0 = \frac{c_p}{c_{psurf}} = \frac{k_{psurf}}{k_p},$$

$$\cosh\theta_0 = \frac{c_s}{c_{ssurf}} = \frac{k_{ssurf}}{k_s},$$

$$\sinh\gamma_0 = \sqrt{\frac{c_p^2}{c_{psurf}^2} - 1}, \qquad \sinh\theta_0 = \sqrt{\frac{c_s^2}{c_{ssurf}^2} - 1}. \tag{43}$$

If the waves

$$\vec{u}_L^R = b\vec{u}_L^{pl}, \qquad \vec{u}_T^R = d\vec{u}_T^{pl}, \tag{44}$$

and they are traveling in a free-traction half-space, the condition $k_{psurf} = k_{ssurf} = k_R \Rightarrow c_{psurf} = c_{svsurf} = c_R$ is obtained, where c_R is the Rayleigh wave velocity. Thus,

$$\cosh\gamma_0 = \frac{c_p}{c_R} = \frac{k_R}{k_p}, \quad \cosh\theta_0 = \frac{c_s}{c_R} = \frac{k_R}{k_s}, \quad \sinh\gamma_0 = \sqrt{\frac{c_p^2}{c_R^2} - 1} = \frac{k_R}{k_p}\sqrt{1 - \frac{c_R^2}{c_p^2}}, \quad \sinh\theta_0 = \sqrt{\frac{c_s^2}{c_R^2} - 1} = \frac{k_R}{k_s}\sqrt{1 - \frac{c_R^2}{c_s^2}}, \tag{45}$$

and

$$\vec{u}_L^R \approx b\left(\frac{k_R}{k_p}\right) e^{-yk_R\sqrt{1-c_R^2/c_p^2}} e^{-ixk_R}\left[\hat{x} - i\sqrt{1 - \frac{c_R^2}{c_p^2}}\hat{y}\right],$$

$$\vec{u}_T^R \approx d\left(\frac{k_R}{k_s}\right) e^{-yk_R\sqrt{1-c_R^2/c_s^2}} e^{-ixk_R}\left[i\sqrt{1 - \frac{c_R^2}{c_s^2}}\hat{x} + \hat{y}\right]. \tag{46}$$

Note that the sum of the expressions in (46), $\vec{u}_R = \vec{u}_L^R + \vec{u}_T^R$, agrees with the expression for a Rayleigh surface wave given by Pujol [16], where, in order to agree with the amplitudes defined by him, $A = b\left(k_R/k_p\right)$ and $B = d(k_R/k_s)$.

In this section, we have shown that the expressions in (38) are surface waves. In Figure-14 the "Geometrical" and "physical" point of view of the inhomogeneous waves in (44) are shown, where $\gamma_0 = \cosh^{-1}\left(\frac{c_p}{c_R}\right)$ and $\theta_0 = \cosh^{-1}\left(\frac{c_s}{c_R}\right)$ with $c_p/c_R > 1$ and $c_s/c_R > 1$, respectively. Furthermore, it can be observed that $\gamma_0 > \theta_0$.

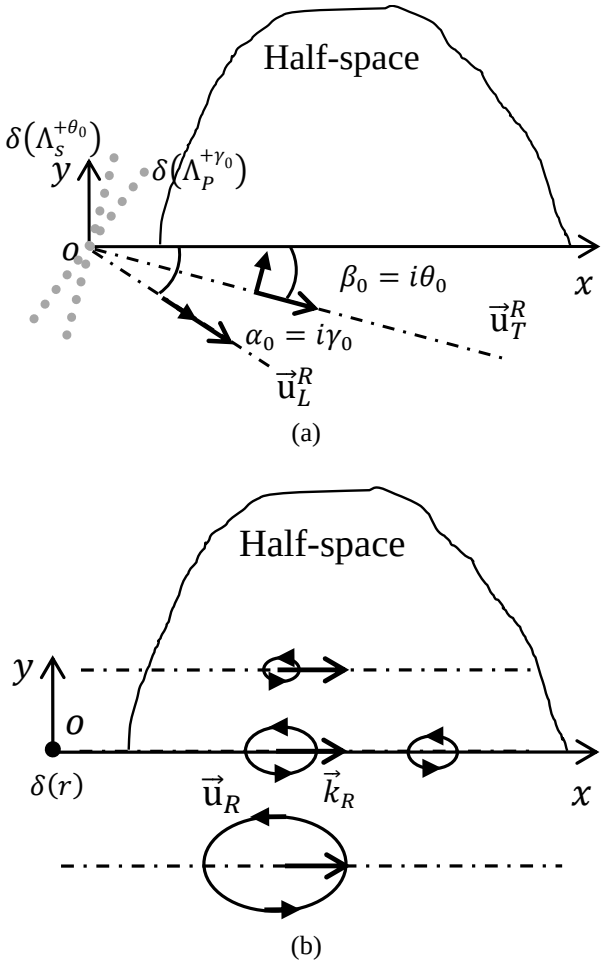

Figure-14. Diagrams in far-field of a Rayleigh wave generated from the sum of *P* and *S* inhomogeneous plane waves for a free-traction half-space: (a) a "Geometrical" point of view and (b) a "Physical" point of view. Plane sources in (a) are imagined and we have drawn it to try to visualize, from a geometrical point of view, the origination of the inhomogeneous plane waves emerging with imaginary angles, since the one real source is a line at the origin.

Finally, considering again the approximations given in section 4.1, it is obtained that

$$\vec{u}_P^{ple} \approx e^{-yk_p\sinh\gamma_0} e^{-ixk_{psurf}}\left\{k_p y\left[\cosh\gamma_0\,\hat{x} + i\left(\frac{1}{k_p y} - \sinh\gamma_0\right)\hat{y}\right]\right\},$$

$$\vec{u}_s^{ple} \approx e^{-yk_s\sinh\theta_0} e^{-ixk_{ssurf}}\left\{k_s y\left[i\left(-\frac{1}{k_s y} + \sinh\theta_0\right)\hat{x} + \cosh\theta_0\,\hat{y}\right]\right\}, \tag{47}$$

where if $\gamma_0 = \theta_0 = 0$ the Goodier-Bishop waves, $\vec{u}_{Py}$ and $\vec{u}_{SVy}$ in (18), are achieved.

6. OTHER SOLUTIONS

In this section, the necessary conditions are defined to obtain expressions that represent waves in terms of the Hankel function. Then, it is defined:

$$\mathcal{G}(r,\phi) = f(r,\phi)H_0^{(2)}(\Lambda), \quad (48)$$

where Λ is the argument of the Hankel function. Now, it is necessary to know what conditions must fulfill $f(r,\phi)$ to satisfy

$$\nabla^2\mathcal{G}(r,\phi) + k^2\mathcal{G}(r,\phi) = 0. \quad (49)$$

First, when $\Lambda = kr$ is analyzed. Replacing (48) in (49), taking into account (3), (11) and the vectorial identity $\nabla^2(\Phi\Psi) = \Phi\nabla^2\Psi + \Psi\nabla^2\Phi + 2\vec{\nabla}\Phi\cdot\vec{\nabla}\Psi$, it is obtained that

$$\nabla^2\mathcal{G} + k^2\mathcal{G} = H_0^{(2)}(\Lambda)\nabla^2 f - 2kH_1^{(2)}(\Lambda)\frac{\partial f}{\partial r} = 0. \quad (50)$$

Finally, considering the approximation (13), the asymptotic condition for large kr is given by:

$$\nabla^2 f(r,\phi) - 2ik\frac{\partial f(r,\phi)}{\partial r} \approx 0. \quad (51)$$

Note that (50) and (51) are fulfilled for $f(r,\phi) = constant$ and $f(r,\phi) = \phi$ which is the particular case (10).

Now, when $\Lambda = kr\cos(\phi \pm \eta_0)$ is analyzed. Therefore,

$$\nabla^2\mathcal{G} + k^2\mathcal{G} = H_0^{(2)}(\Lambda)\nabla^2 f - 2kH_1^{(2)}(\Lambda)\left(\cos\phi\frac{\partial f}{\partial r} - \frac{\sin\phi}{r}\frac{\partial f}{\partial\phi}\right) = 0, \quad (52)$$

and considering again (13), it is achieved that

$$\frac{1}{k^2}\nabla^2 f(r,\phi) - \frac{2i}{k}\left(\cos\phi\frac{\partial f(r,\phi)}{\partial r} - \frac{\sin\phi}{r}\frac{\partial f(r,\phi)}{\partial\phi}\right) \approx 0. \quad (53)$$

It can also be observed that

$$f(r,\phi) = 1/\Lambda^j,$$

$$f(r,\phi) = \phi/\Lambda^j, \quad (54)$$

with $j > 0$, fulfill (51) and (53) for large Λ. Then,

$$\mathcal{G}(r,\phi) = \frac{1}{\Lambda^j}H_0^{(2)}(\Lambda)\left[A_j\phi + B_j\right], \quad (55)$$

with $\Lambda = kr$ or $\Lambda = kr\cos(\phi \pm \eta_0)$, are asymptotic solutions of (3), where A_j and B_j are complex constants in general.

7. DISCUSSION AND CONCLUSIONS

In this paper some exact and asymptotic analytical solutions of the displacement equation have been studied, considering the most general solution of the Helmholtz equation. These solutions are not shown in papers and standard texts, for instance [11, 14, 15, 16]. Equations (12) and (18) are exact solutions of (1),which is unexpected because (18) were obtained after applying a series of approximations to (12), (26), (30) and (38).In (18) the main disadvantage is that the waves do not regard a generating origin (this is equivalent to consider plane waves from infinity) and they are valid near to the half-space surface, producing a local solution [13, 14], in contrast with (12), (26), (30) and (38) that are valid solutions for all space. It is also shown that (19) are potentials that generate homogeneous (see (25) and (29)) and inhomogeneous plane waves (see (30), (36), (38) and (43)). Moreover, the authors have tried to give a meaning to all these expressions, from a geometrical point of view, for a better conceptualization of these solutions.

The solutions presented in this work can be combined with other known waves in order to satisfy boundary conditions in *P-S* waves problems such as in [11, 13, 14, 16] (see (18), (35) and (36), (45) and (46)); which is a good strategy for understanding complex problems due to the fact that the solution is divided into parts that can be manipulated and interpreted more easily, and furthermore, used in other problems.

Conditions (49)-(52) permit to find either exact or approximated solutions of $f(r,\phi)$, therefore multiplying it by the Hankel Function the equations in (3) are fulfilled. This provides an alternative way to find solutions, which could be helpful when $f(r,\phi)$ is simple such as in (54). We can also observe that (55) could be taken as ansatz functions to develop approximate analytical solutions by series expansions along with other known solutions, particularly for matching boundary conditions. These kinds of analysis are going to be reported in future works.

ACKNOWLEDGMENT

V. H. A. gives thanks to Belizza J. Ruiz and Francisco J. Velez for the critical reading of the manuscript and useful suggestions. Also he acknowledges financial support granted by Colciencias through the program for national Ph.D. students.

REFERENCES

[1] Trifunac M.D. 1971. Surface motion of a semi-cylindrical alluvial valley for incident plane SH waves. Bull. Seism. Soc. Am. 61(6): 1755-1770.

[2] Trifunac M.D. 1974. Scattering of plane SH waves by a semi-cylindrical canyon. Earthq. Eng. and Struct. Dyn.1, 267-281.

[3] Wong H.L., Trifunac M.D. 1974. Scattering of plane SH waves by a semi-elliptical canyon, Earthq. Eng. and Struct. Dyn. 3, 157-169.

[4] Wong H.L., Trifunac M.D. 1974. Surface motion of a semi-elliptical alluvial valley for incident plane SH waves. Bull. Seism. Soc. Am. 64, 1389-1408.

[5] Sanchez-Sesma F.J. 1985. Diffraction of elastic SH waves by wedges. Bull. Seism. Soc. Am. 75(5): 1435-1446.

[6] Todorovska M.I., Lee V.W. 1991. Surface motion of shallow circular alluvial valleys for incident plane SH waves-analytical solution. Soil Dyn. and Earthq. Eng. 10(4): 192-200.

[7] Yuan X.M., Men F.L. 1992. Scattering of plane SH waves by a semi-cylindrical hill. Earthq. Eng. and Struct. Dyn.21, 1091-1098.

[8] Lee V.W. 1982. On note on scattering of elastic plane waves by a hemispherical canyon. Soil Dyn. and Earthq. Eng. 1(3): 122-129.

[9] Lee V.W. 1984. Three-dimensional diffraction of plane P, SV and SH waves by a hemispherical alluvial valley. Soil Dyn. and Earthq. Eng. 3(3): 133-144.

[10] Todorovska M.I., Lee V.W. 1990.A note on response of shallow circular valleys to Rayleigh waves: analytical approach. Earthq. Eng. and Eng. Vib. 10(1): 21-34.

[11] Achenbach J.D. 1973. Wave Propagation in Elastic Solid. North-Holland Publishing Company, Amsterdan, London, U.K.

[12] Abramowitz M., StegunI.A. 1965. Handbook of Mathematical Functions. 9th printing, U.S. Government Printing Office, Washington, D.C., USA.

[13] Goodier J.N., Bishop R.E.D. 1952. A note on critical reflections of elastic waves at free surface. J. Appl. Phys. 23(1): 124-126.

[14] Graff K. 1991. Wave Motion in Elastic Solid, chapter 6. Dover Publication, INC., New York, USA.

[15] Eringen A.C., Suhubi E.S. 1975. Elastodynamics Vol. II, section 7.5. Academic Press, INC., New York, USA.

[16] Pujol J. 2003. Elastic Wave Propagation and Generation in Seismology, Section 7.4.1. Cambridge University Press, New York, USA.

APPENDIX 1

First, the next function is defined

$$\mathcal{G}(r,\phi) = \Psi(\Lambda)[A\phi + B],$$

where $\Lambda = kr\cos(\phi \pm \eta_0)$. Second, we use the vectorial identity

$$\nabla^2(\Phi\Psi) = \Phi\nabla^2\Psi + \Psi\nabla^2\Phi + 2\vec{\nabla}\Phi\cdot\vec{\nabla}\Psi$$

with $\Phi = A\phi + B$. Third, the Laplacians and Gradients in Polar coordinate of $\Psi(\Lambda)$ and Φ are calculated:

$$\nabla^2\Psi(\Lambda) = k^2\frac{\partial^2\Psi(\Lambda)}{\partial\Lambda^2},$$

$$\nabla^2\Phi = 0,$$

$$\vec{\nabla}\Phi\cdot\vec{\nabla}\Psi(\Lambda) = -\frac{Ak\sin\phi}{r}\frac{\partial\Psi(\Lambda)}{\partial\Lambda}.$$

Now, we replace in the previous vectorial identity

$$\nabla^2\mathcal{G} = \nabla^2(\Phi\Psi) = k^2[A\phi + B]\frac{\partial^2\Psi(\Lambda)}{\partial\Lambda^2} - 2\frac{Ak\sin\phi}{r}\frac{\partial\Psi(\Lambda)}{\partial\Lambda}.$$

Finally, we reorganize

$$\nabla^2\mathcal{G} - k^2[A\phi + B]\frac{\partial^2\Psi(\Lambda)}{\partial\Lambda^2} + 2\frac{Ak\sin\phi}{r}\frac{\partial\Psi(\Lambda)}{\partial\Lambda} = 0.$$